Diffusion Foundations Vol 5 (2015) pp 95-108

doi:10.4028/www.scientific.net/DF.5.95

Diffusion and Phase Transitions Accelerated by Severe Plastic Deformation

Boris B. Straumal[1-3,a *], Olga A. Kogtenkova[1,b], Ruslan Z. Valiev[4,5c], Pawel Zięba[6,d] and Brigitte Baretzky[2,e]

[1]Institute of Solid State Physics, Russian Academy of Sciences, Ac. Ossipyan str. 2, 142432 Chernogolovka, Russia

[2]Karlsruhe Institute of Technology (KIT), Institute of Nanotechnology, Hermann-von-Helmholtz-Platz 1, D-76344 Eggenstein-Leopoldshafen, Germany

[3]Laboratory of Hybrid Nanomaterials, National University of Science and Technology "MISIS", Leninski prosp. 4, 119049 Moscow, Russia

[4]Institute for Physics of Advanced Materials, Ufa State Aviation Technical University, Karl Marx str. 12, 450000 Ufa, Russia

[5]St. Petersburg State Polytechnical University, Polytechnicheskaya str. 29, Saint Petersburg 195251, Russia

[6]Institute of Metallurgy and Materials Science, Polish Academy of Sciences, Reymonta St. 25, 30-059 Cracow, Poland

[a]straumal@issp.ac.ru, [b]koololga@issp.ac.ru, [c]rzvaliev@mail.rb.ru, [d]p.zieba@imim.pl, [e]brigitte.baretzky@kit.edu

*corresponding author

Keywords: severe plastic deformation, phase transformations, high-pressure torsion, effective temperature.

Abstract. Severe plastic deformation (SPD) can lead to the phase transformations in the materials. Even the SPD-treatment at ambient temperature T_{SPD} = 300 K is frequently equivalent to the heat treatment at a certain elevated temperature (effective temperature) T_{eff} > 300 K. However, if the real annealing at effective temperature leads to the grain growth, SPD leads to strong grain refinement. SPD also accelerates the mass transfer in the materials. In this review the methods of determination for effective temperature after high-pressure torsion of metallic alloys are discussed as well as SPD-driven acceleration of diffusion.

Introduction

Severe plastic deformation (SPD) is a novel and powerful method in the hands of metallurgists and engineers for tailoring the structure and properties of materials [1]. The idea of SPD is to deform the material in a confined space. It permits to increase the strain up to enormous values without fracture of a material. SPD frequently leads to the phase transformations in the materials [2, 3] e.g. the formation [4–12] or decomposition [13–15] of a supersaturated solid solution, dissolution of phases [16–28], disordering of ordered phases [19–31], amorphization of crystalline phases [32–40], synthesis of the low-temperature [21,28], high-temperature [41–43] or high-pressure [44–52] allotropic modifications, and nanocrystallization in the amorphous matrix [53–61]. Quite frequently, the phases after SPD are the same as phases which would appear in a material after long anneal at a certain (elevated) temperature. This temperature is called effective temperature T_{eff}. It has been demonstrated recently that concept of effective temperature T_{eff} originally proposed for the materials under severe irradiation [62] is applicable also for severe plastic deformation (SPD) [63]. If the atomic movements driven by an external action (deformation or irradiation) are higher in comparison with the conventional thermal diffusion, the material is forced to undergo into a state which is equivalent to that at a certain increased (effective) temperature T_{eff}. One can estimate T_{eff} if

the phases in a material after SPD treatment differ from those before SPD [63]. For the determination of T_{eff} one can use also the phase diagrams at high pressures, if they are known [44–52]. However, the SPD-treatment at ambient temperature T_{SPD} usually leads to the very quick phase transformations, which is easy to understand if one considers the high density of defects, similar to an increased temperature. The increased pressure, oppositely, leads to the decrease of diffusivity and/or grain boundary mobility [64,65]. Some SPD-driven phase transformations need only a small shift of atoms, for other ones the long-range mass transfer is needed. The results of such SPD-driven transitions cannot be explained by the bulk or even grain boundary diffusion at the SPD temperature (which usually remains slightly above ambient one). In this review the methods of T_{eff} determination of metallic alloys after high-pressure torsion are discussed. For the determination of T_{eff} we choose the alloys where the phases after HPT strongly differ from the ones before HPT. The alloys studied have also well investigated and unambiguously known equilibrium phase diagrams. These phase diagrams allowed us the easy comparison with observed phases after SPD and, therefore, easy and reliable determination of T_{eff}. We also discuss the accelerated mass transfer during SPD. The results of the SPD-driven phase transformations allow one to estimate the diffusion coefficients equivalent to the SPD-driven mass transfer.

Determination of Effective Temperature

The atom movements caused by strong external forces can drive both accelerated diffusion and phase transformations in the material. Historically, such unusual behaviour was first observed in materials under severe irradiation [62]. G. Martin proposed a simplified mean-field description of solid solutions subjected to irradiation-induced atomic mixing [62]. His main idea was that the forced mixing induced by irradiation emulates the increase of entropy and changes the thermodynamic potentials in the alloy. In a simple case of regular solution in the Bragg-Williams approximation, a law of corresponding states was formulated: The equilibrium configuration of the solid under irradiation flux φ at temperature T is identical to the configuration at φ = 0 and a certain effective temperature

$$T_{eff} = T(1+\Delta). \quad (1)$$

If the irradiation-driven movements of atoms are similar in amplitude to conventional diffusion jumps, they can be described by the "ballistic" diffusion coefficient D_{ball} and $\Delta = D_{ball}/D_b$, where D_b is conventional bulk diffusion coefficient, possibly increased due to the non-equilibrium defect concentration [62]. It means that one can use the equilibrium phase diagram for the description of the system under irradiation, but at T_{eff} instead of the actual temperature T. For example, if the liquid phase is present in the phase diagram at T_{eff}, the amorphous phase would appear under irradiation [62, 66].

To check the applicability of the Martin's law (1) to the forced diffusion driven by pure shear deformation (D_{HPT}) instead of irradiation (D_{ball}), experiments where HPT leads to the phase transformations have to be analyzed. We have chosen for the comparison the data where (i) the HPT-driven atomic movements are comparable with each other, i.e. HPT was performed at 4-6 GPa with 4-6 torsions and (ii) the phases appeared after HPT can be easily localized in the phase diagrams and are different from those present in the samples before HPT.

The supersaturated solid solution in the as-cast Al–30 wt.% Zn alloy contained about 15 wt.% Zn (Fig. 1, filled square) [13,14,67]. The as-cast Al–20 wt.% Zn and Al–10 wt.% Zn alloy contained about 7 and 3 wt.% Zn in the supersaturated solid solution. The HPT at room temperature produced nanograined pure Al and pure Zn particles (filled circles) simultaneously leading to unusual softening [13,14]. In other two as-cast alloys the supersaturated solid solution also completely decomposed, and the lattice spacing in all three alloys became indistinguishable from that of pure aluminium. The respective T_{eff} = 30°C (Fig. 1). The decomposition during SPD proceeds extremely quickly, already after about 0.5 rotations of anvils the lattice spacing becomes equal to that of Al and microhardness reaches its stationary value [67].

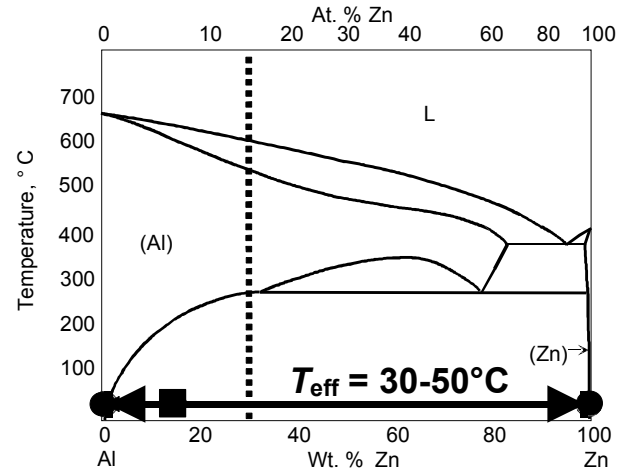

Fig. 1. Al–Zn phase diagram [68]. Vertical dotted line shows the composition of Al–30 wt.% Zn alloy. Filled square shows the composition of supersaturated (Al) solid solution in coarse-grained Al–30 wt.% Zn alloy before HPT. Filled circles show the composition of phases in ultra-fine-grained Al– 30 wt.% Zn alloy after HPT [13]. The value of T_{eff} = 30-50°C is also given.

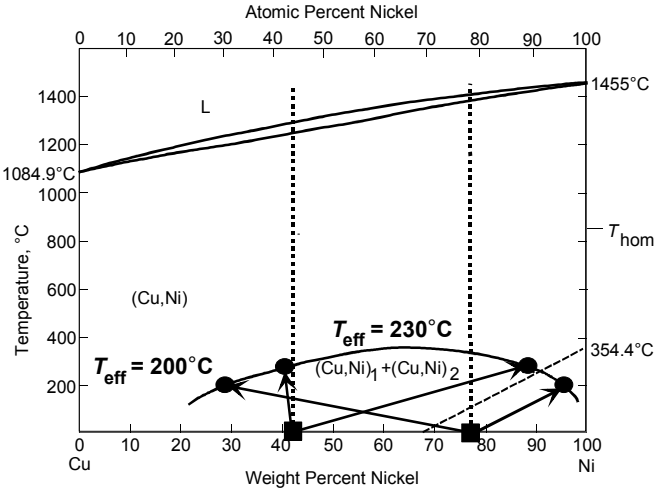

Fig. 2. Cu–Ni phase diagram [68]. Vertical dotted lines shows the composition of Cu–42 wt.% Ni and Cu–77 wt.% Ni alloys. Filled squares show the compositions of supersaturated (Cu) solid solutions in coarse-grained Cu–42 wt. % Ni and Cu–77 wt.% Ni alloys before HPT. They correspond with overall composition of both alloys. Filled circles show the composition of phases in ultra-fine-grained Cu–42 wt.% Ni and Cu–77 wt.% Ni alloys after HPT [15]. The values of T_{eff} = 200°C for the Cu–77 wt.% Ni alloy and T_{eff} = 230°C for the Cu–42 wt.% Ni alloy are also given.

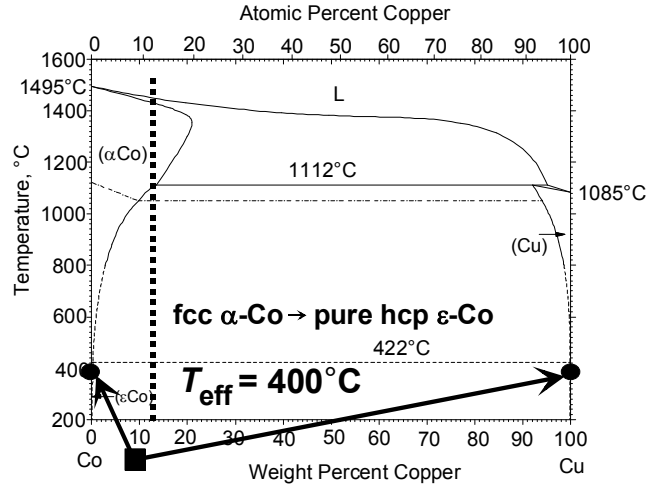

Fig. 3. Co–Cu phase diagram [68]. Vertical dotted line shows the composition of Co–12 wt.% Cu alloy. Filled square shows the composition of supersaturated (Co) solid solution in coarse-grained Co–12 wt.% Cu alloy before HPT. It contains fcc α-Co phase. Filled circles show the composition of phases in ultra-fine-grained Co–12 wt.% Cu alloy after HPT (pure hcp ε-Co and pure Cu) [63]. The value of T_{eff} = 400°C is also given.

The homogenized one-phase solid solutions in the Cu–Ni alloys with 42 and 77 wt. % Ni decomposed after HPT at room temperature into Cu-rich and Ni-rich phases (Fig. 2) [15]. The composition of resulting phases (filled circles) permitted an estimation of T_{eff} = 200°C for the Cu–77 wt.% Ni alloy and T_{eff} = 270°C for the Cu–42 wt.% Ni alloy (Fig. 2) [15].

In case of Co-rich Co–Cu alloys, the as-cast Co–12 wt.% Cu alloy contained the supersaturated solid solution with 8 wt.% Cu in the Co matrix with fcc α-structure (Fig. 3) [63]. After HPT, together with grain refinement, the full decomposition of supersaturated (Co) solid solution proceeds. In addition, the high-temperature fcc α-Co transformed into low-temperature hcp ε-Co (Fig. 3). The respective T_{eff} = 400°C for the Co–Cu system (Fig. 3) [2].

In Cu-rich Co–Cu alloys the situation is even more interesting [69]. The Cu–4.9 wt. % Co alloy has been subjected to high pressure torsion in two different states, namely with Co fully dissolved in the Cu-rich matrix (after annealing at 1060°C for 10 h, Sample 2) and fully precipitated from the Cu matrix (after annealing at 570°C for 840 h, Sample 1). With an increasing number of rotations, the lattice parameter of Sample 1 decreased and that of Sample 2 increased. After 5 anvil rotations (1800 deg.) the lattice parameter in both samples becomes almost undistinguishable and corresponds to the solid solution of Co in Cu with 2.5 wt.%. In other words, the composition of the solid solution in the Cu – 4.9 wt. % Co alloy after the given HPT processing does not depend on the initial state prior to HPT. Thus, the steady-state with respect to the grain size, size of Co precipitates and concentration of Co in a solid solution during HPT is indeed *equifinal*. The composition of Cu-rich matrix in both alloys before and after HPT is shown in the Cu–Co phase diagram (Fig. 4). The solid solution in samples 1 and 2 after HPT contains as much Co, as if they would be annealed at T_{eff1} = 920±30°C and T_{eff2} = 870±30°C, respectively.

Six Cu–In alloys with 2.3, 4, 5.8, 7, 9.5 and 13.5 at.% In have been studied in [70]. The Cu–In alloys possess the negative mixing enthalpy. The torsion torque during HPT reached a steady-state after 1-2 anvil rotations. Differently to the alloys with positive mixing enthalpy, the Cu(In) solid solution in the samples2.3, 4, 5.8, 7, and 9.5 at.% In with did not decompose. However, the precipitates of δ-phase in the Cu–13.5 at. % In alloy partially dissolved and additionally enriched the Cu(In) solid solution (Fig. 5). As a result, the concentration of indium in the Cu-matrix becomes at least as high as a sample annealed at T_{eff} = 574°C (Fig. 5).

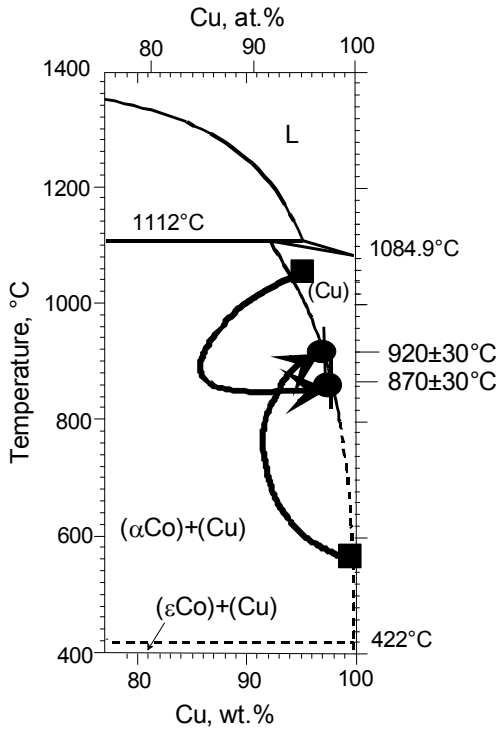

Fig. 4. The Cu-rich part of the Co–Cu phase diagram [68]. The composition of Cu-rich matrix in both alloys before (squares) and after (circles) HPT is shown.

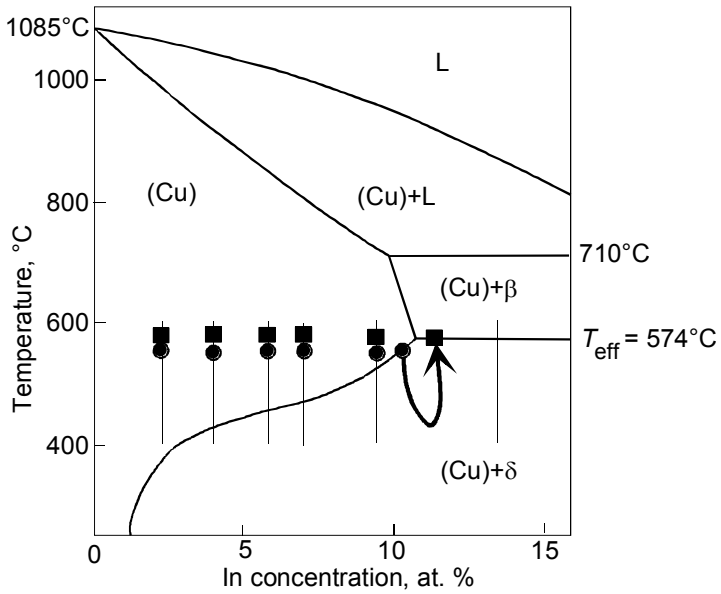

Fig. 5. The Cu-rich part of the Cu–In phase diagram [68]. Thin vertical lines show the In concentration in the studied alloys. Squares show the concentration in the Cu-matrix HPT and circles show the concentration in the Cu-matrix after HPT. T_{eff} = 574°C

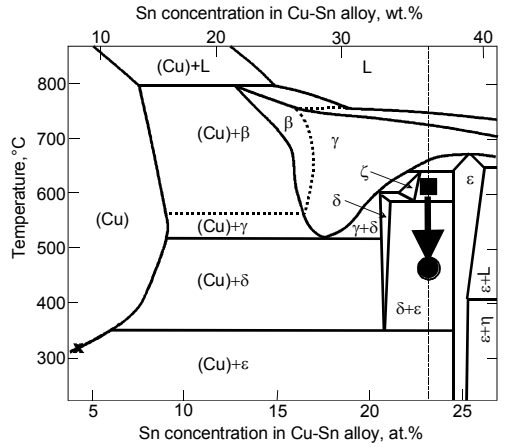

Fig. 6. Part of the phase diagram of Cu–Sn [68]. The thick solid and thick dashed lines correspond to first and second order phase transitions, respectively. The vertical dashed line indicates the alloy under study. The filled square and filled circle indicate the phase compositions of the as cast alloy before and after high pressure torsion, respectively.

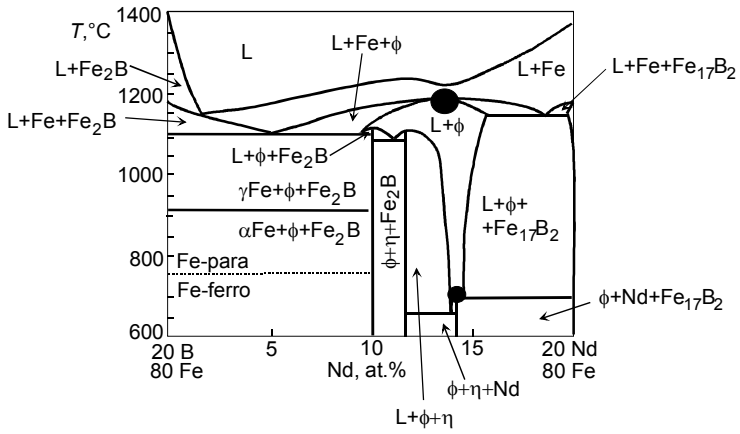

Fig. 7. The 80 at.% Fe section of the Nd–Fe–B phase diagram [73–76]. Large filled circle shows the effective temperature T_{eff} = 1170±30 °C for the Nd–Fe–B-based alloy (66.5 wt.% Fe, 22.1 wt.% Nd, 9.4 wt.% Dy, 1.0 wt.% Co, 0.8 wt.% B, 0.2 wt.% Cu) [72]. Small filled circle shows the effective temperature T_{eff} = 700 °C for the Fe–20 wt.% (Nd,Pr)–5 mass % B–1.5 wt.% Cu alloy [16].

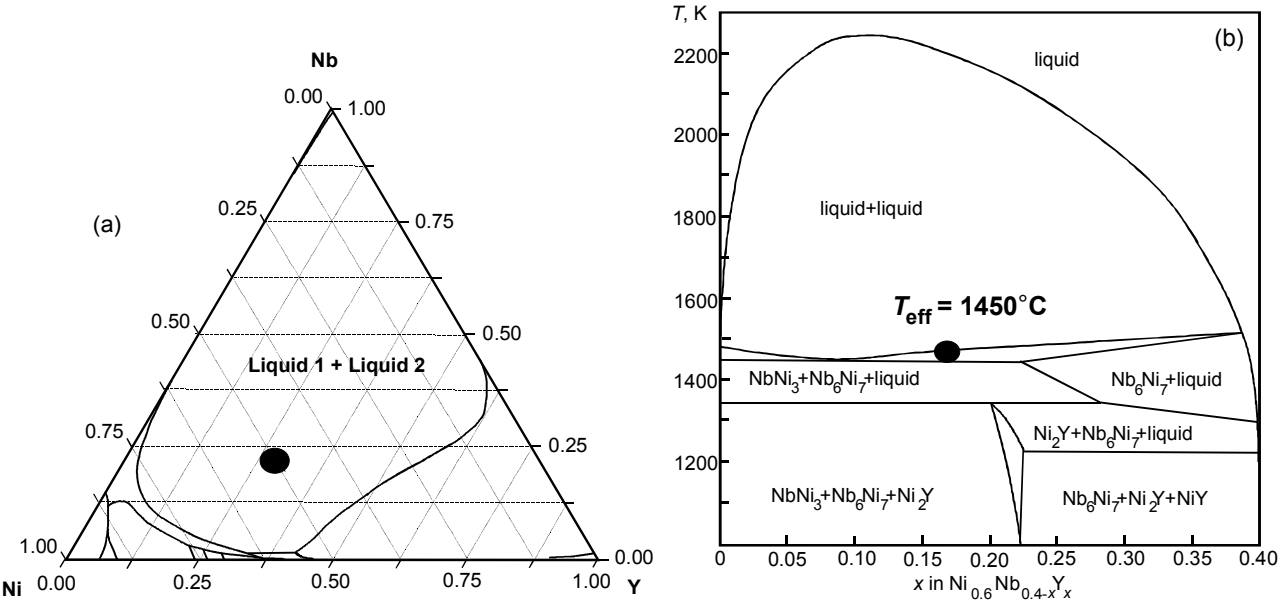

Fig. 8. (a) Liquidus projection obtained by the CALPHAD method of the Y–Ni–Nb ternary phase diagram at [77]. The composition of the triple $Ni_{50}Nb_{20}Y_{30}$ alloy used for HPT investigations is marked by the large black circle. (b). Calculated pseudo-binary section of the ternary phase diagram $Ni_{60}Y_{40}$–$Ni_{60}Nb_{40}$ [78]. Large grey circle shows the composition of phases in ultra-fine-grained alloy after HPT (two amorphous phases and two crystalline ones) [36, 39]. The value of T_{eff} = 1450°C is also given.

It has been also revealed that high pressure torsion induces phase transformations of certain Hume-Rothery phases (electron compounds) to others [71]. High pressure torsion induces the ζ → δ + ε reaction in copper–tin alloys with the appearance of the δ + ε phase mixture as after long term annealing in the temperature range T_{eff} = 350–589°C (Fig. 6).

The Fe–20 wt.% (Nd,Pr)–5 mass % B–1.5 wt.% Cu alloy containing crystalline phases [$(Nd,Pr)_2Fe_{14}B$ and Pr-rich phase] transforms after HPT into a mixture of the amorphous phase and $(Nd,Pr)_2Fe_{14}B$ nanograins [16]. According to the Martin's model this means that the T_{eff} is so high that the configurative point for the treated alloy is in the two-phase area where both solid and liquid phases are present. The melt appears in the Nd–Fe–B system above eutectic temperature T_e = 665°C [17]. It means that the effective temperature is slightly above T_e = 665°C and can be estimated as T_{eff} = 700°C (Fig. 7, small filled circle). In case of Nd–Fe–B-based alloy (66.5 wt.% Fe, 22.1 wt.% Nd, 9.4 wt.% Dy, 1.0 wt.% Co, 0.8 wt.% B, 0.2 wt.% Cu) HPT leads to the formation of two amorphous phases [72]. The Nd–Fe–B phase diagram contains two immiscible melts above 1150°C [73–76] (Fig. 7). Therefore, the effective temperature is slightly above 1150°C and can be estimated as T_{eff} = 1170±30°C (Fig. 7, large filled circle).

The coarse-grained as-cast Ni–20 wt.% Nb–30 wt.% Y and Ni–18 wt.% Nb–22 wt.% Y alloys contained before HPT the NiY, $NbNi_3$, Ni_2Y, Ni_7Y_2 and Ni_3Y phases (Fig. 8a) [36, 39]. After HPT these alloys transformed into a mixture of two nanocrystalline NiY and $Nb_{15}Ni_2$ phases and two different amorphous phases (one was Y-rich and another Nb-rich). The Ni–Nb–Y phase diagram contains two immiscible melts above 1440°C [66]. Therefore, the effective temperature is slightly above T_e = 1440°C and can be estimated as T_{eff} = 1450°C (Fig. 8). It is remarkable that the rapid solidification of these alloys from the liquid state also allows obtaining the mixture of two amorphous phases.

Accelerated Diffusion

The discussed phase transformations (dissolution and formation of precipitates, amorphisation, transitions between Hume-Rothery phases etc.) are connected with redistribution of components and, therefore, with mass transfer. This SPD-driven mass transfer proceed extremely quickly (usual time for establishment of steady-state by HPT is only 2-5 minutes) and at ambient temperature without substantial increase of temperature. Let us estimate the observed SPD-driven mass-transfer using the effective diffusion coefficient and compare it with "conventional" diffusion coefficients at temperature of HPT-treatment and at T_{eff}.

The supersaturation in solid solution is the driving force for the bulk diffusion (mass transfer) of Zn and Mg in the Al–Zn and Al–Mg alloys from the solid solution to the sinks which are the particles of (Zn) and β-phase (Al_3Mg_2), respectively [13]. We can suppose that the average diffusion path, L, for individual Zn and Mg atoms during HPT-treatment atoms can be estimated as grain size in Al–Zn and Al–Mg alloys after HPT. They would be about 800 and 100 nm, respectively. Thus we can estimate the value of D_{HPT} which ensures the decomposition of a supersaturated solid solution employing an approximate relationship $L \approx (D_{HPT}t)^{0.5}$ (t = 300 s being the HPT treatment duration). D_{HPT} corresponds to the bulk diffusion coefficients of 10^{-15} m^2s^{-1} for Zn and 10^{-17} m^2s^{-1} for Mg. There are two groups of tracer diffusion data for bulk diffusion of Zn in Al: measured in polycrystals (D_0 = 0.30 10^{-4} m^2s^{-1}, Q = 121.4 $kJmol^{-1}$, obtained within the range 700–920 K, ^{65}Zn, [79]) and single crystals (D_0 = 0.259 10^{-4} m^2s^{-1}, Q = 120.8 $kJmol^{-1}$, 630–926 K, ^{65}Zn [80]). After the extrapolation to 300 K (being the temperature of HPT treatment) the both data yield very close values of D (300 K) = 0.95 10^{-23} m^2s^{-1} and D (300 K) = 1.0 10^{-23} m^2s^{-1}. This is about 8 orders of magnitude less than the value estimated from the diffusion path of the actual solid-solution decomposition during HPT. Extrapolation of the data for Mg bulk diffusion in Al single crystals (D_0 = 1.24 10^{-4} m^2s^{-1}, Q = 130.4 $kJmol^{-1}$, 667–928 K, ^{28}Mg [81]) gives D (300 K) = 1.7 10^{-24} m^2s^{-1}. It means that though Mg diffuses slower than Zn, the difference of about 8 orders of magnitude remains unexplained.

Let us compare the HPT-driven mass transfer with possible input of grain boundary diffusion. In Al–Zn alloys the supersaturated solid solution with concentration of ~ 12 wt. % completely decomposes after 300 s. The mean distance between Zn particles in the nanostructured Al–30 wt. % Zn alloy is about 2 μm. It means that each particle collected the Zn atoms from the surrounding area

with a radius (diffusion path) of about 2 μm. This area includes several (Al) grains and many (Al) GBs. If this process would be controlled by bulk diffusion, D_{HPT} could be estimated as $D_{HPT} = (10^{-12}$ m^2/ 300 s) = 3 10^{-15} m^{2}s^{-1} which is at least 8 orders of magnitude higher than D for conventional bulk diffusion at 300 K. The transport of Zn from the (Al) matrix can be controlled by grain boundary diffusion of Zn atoms along (Al) GBs. Let us suppose that the moving GBs during HPT swept at least once each Zn atom in the bulk, and then bulk diffusion towards GB has not to be considered. In this case the path for GB diffusion would be roughly 1 μm yielding $sD\delta$ value of 1.5 10^{-24} m^{3}s^{-1} for a GB thickness of δ = 0.5 nm and a segregation factor s = 1.

In [82] the data were obtained for ^{65}Zn tracer GB diffusion in the 99.99% purity Al polycrystal within the temperature interval 428–593K. Three groups of GBs were defined, namely (I) high-angle GBs with high activation energy Q of GB diffusion ($sD_0\delta$ = 1 10^{-9} m^{3}s^{-1}, Q = 118 kJmol^{-1}), (II) high-angle GBs with low activation energy ($sD_0\delta$ = 1.6 10^{-11} m^{3}s^{-1}, Q = 90 kJmol^{-1}) and (III) low-angle GBs between subgrains ($sD_0\delta$ = 6 10^{-14} m^{3}s^{-1}, Q = 60 kJmol^{-1}). Extrapolation of these data to 300 K yield, respectively, (I) $sD\delta$ = 3 10^{-24} m^{3}s^{-1}, (II) $sD\delta$ = 2 10^{-26} m^{3}s^{-1}, and (III) $sD\delta$ = 2 10^{-29} m^{3}s^{-1}. The first value is surprisingly close to the estimation for the diffusion path needed to the equilibration of the Al–Zn supersaturated solid solution during the HPT treatment. A similar value of $sD\delta = 10^{-23}$ m^{3}s^{-1} obtains also from [83, 84].

In [85] the parameters of Zn GB diffusion were measured by electron probe microanalysis in Al bicristals with individual tilt and twist GBs with various misorientation angles within the interval 523–613 K. The pre-exponentials $sD_0\delta$ and activation energies Q for tilt GBs lie within the intervals 2 10^{-16}–10^{-12} m^{3}s^{-1} and 40–80 kJmol^{-1} respectively [85]. The pre-exponentials and activation energies for twist GBs are within the intervals 10^{-15}–10^{-9} m^{3}s^{-1} and 50–130 kJmol^{-1} respectively [86]. The extrapolation to 300 K yields $sD\delta$ values for tilt GBs between 10^{-24} and 10^{-22} m^{3}s^{-1}. Therefore, all tilt GB studied in [85] and some twist GBs form a family of "high-diffusivity" GBs which can build channels for the diffusion which is fast enough to equilibrate the Al–Zn solid solutions during HPT.

In [87] the parameters of Zn GB diffusion were determined in an Al–30 wt.% Zn alloy using the discontinuous precipitation reaction controlled by GB diffusion. The advantage of these measurements is that they were performed at rather low temperatures of 350–500 K. Extrapolation to 300 K yields a $sD\delta$ value of 4 10^{-23} m^{3}s^{-1}. Therefore, the GBs in Al provide the diffusion paths for Zn which can be responsible for the decomposition of supersaturated solid solution during HPT. The ^{65}Zn tracer measurements obtained in the temperature interval 493–673 K demonstrate that the increase of the Zn content can further enhance the GB diffusivity in Al–Zn alloys [88–90]. The extrapolation to 300 K yields $sD\delta$ values of 3 10^{-22} m^{3}s^{-1} (2 wt.% Zn), 10^{-21} m^{3}s^{-1} (4.33 wt. % Zn) and 10^{-20} m^{3}s^{-1} (8 to 10 at. % Zn).

Data on Mg GB diffusion in Al are not so numerous, maybe due to the lower values of $sD\delta$. Values of $sD_0\delta$ = 7 10^{-14} m^{3}s^{-1} and Q = 87 kJmol^{-1} were obtained in [91, 92]. The extrapolation to 300 K yields $sD\delta$ value of 5 10^{-28} m^{3}s^{-1}. It is about 5 orders of magnitude lower than the typical values for the Zn GB diffusivity. Direct comparison of Zn and Mg diffusion allow the data on chemical diffusion in Al–0.1 wt. % Sc alloys [93]. Though the $sD\delta$ values were extracted from the comparison of integral measurements on coarse- and nanograined polycrystals obtained by ECAP (as well as in [91, 92]), the data demonstrate undoubtedly a lower GB diffusivity of Mg in comparison with Zn. This fact can explain the slower decomposition of supersaturated solid solution in Al–Mg alloys studied in present work in comparison with Al–Zn alloys deformed in the same HPT conditions. Nevertheless, both Zn and Mg GB diffusivities extrapolated towards 300 K are much higher than the $sD\delta$ value for the Al GB self-diffusion (10^{-31} m^{3}s^{-1} [84]). Based on (unfortunately rather scarce) data on GB diffusion in Al, one can expect that Al–Ga supersaturated solid solutions would also decompose very quickly ($sD\delta$ value extrapolated to 300 K is about 10^{-21} m^{3}s^{-1} [94]).

If GB diffusion is so effective, why the supersaturated solid solution does not decompose without any HPT? The reason is in the low bulk diffusivity. The solute atoms are frozen in the bulk and cannot reach the GBs. During HPT GBs move, sweeping in such a way the "frozen" solute atoms. This mechanism is to a certain extent opposite to the well-known diffusion induced grain boundary migration (DIGM).

In case of decomposition of Cu–Ni alloys [15] the average grain size after HPT is about 100 nm. The approximate relationship $L \approx (D_{HPT}t)^{0.5}$ (t = 300 s being the HPT treatment duration) yields $D_{HPT} = 3\times10^{-17}$ m^2/s. In our opinion, it is unlikely that the bulk interdiffusion is responsible for decomposition during the HPT processing. Indeed, the range of bulk chemical interdiffusion coefficients in the Cu–Ni alloys at room temperature can be estimated by impurity diffusion coefficients of Ni in Cu, D_{Cu}^{Ni} and Cu in Ni, D_{Ni}^{Cu}. Extrapolating the literature data to the room temperature (27°C) yields $D_{Cu}^{Ni} = 4.8\times10^{-44}$ m^2/s and $D_{Ni}^{Cu} = 2.3\times10^{-49}$ m^2/s [95]. These diffusivities can be significantly increased by the non-equilibrium excess vacancies produced during HPT. Assuming that the highest vacancy concentration that a solid can sustain corresponds to the equilibrium vacancy concentration at the melting temperature, and with literature values of vacancy formation enthalpies of 1.28 eV and 1.88 eV for Cu and Ni, respectively [96], we estimate the maximal room temperature diffusivities as $D_{Cu}^{Ni} = 3\times10^{-27}$ m^2/s and $D_{Ni}^{Cu} = 3\times10^{-23}$ m^2/s. These values are still 6 to 10 orders of magnitude lower than our estimate $D = 3\times10^{-17}$ m^2/s. The external pressure can additionally slow down the diffusion [64, 65]. At the same time, extrapolating the diffusion coefficients along the "ultrafast" GBs measured recently in the pure Ni [97] and Cu–Zr alloy [98] processed by equal channel angular pressing (ECAP) yields the room temperature GB diffusivities in the range of 3×10^{-20} m^2/s. This is closer to our estimate of $D = 3\times10^{-17}$ m^2/s, with the remaining difference of three orders of magnitude being possibly associated with the uncertainties in determining D, the differences between the ECAP and HPT processes, and with the fact that diffusion measurements in Refs. [97, 99] were performed after the ECAP process, so that a significant part of non-equilibrium defect had a time to annihilate. In conclusion, simple estimates presented above lend credibility to the hypothesis that the GB, rather than bulk interdiffusion controls the decomposition process in the Cu – 42 wt.% Ni and Cu – 77 wt.% Ni alloys.

Substituting in Eq. (1) our estimate $D = 3\times10^{-17}$ m^2/s yields $D_{Ball} = D_{HPT} = 2.4\times10^{-17}$ m^2/s for the "ballistic" interdiffusion coefficient. The physical mechanism of the intermixing induced by plastic shear is a roughening of the bi-material interface [99]. This roughening is kinematic in nature (i.e. controlled mainly by slip geometry), and is a weak function of the other material constants. This provides an explanation why in the Al–Zn alloys the effective temperature of HPT was close to the room temperature. Indeed, the chemical interdiffusion coefficient in Al–Zn is many orders of magnitude higher than that in Cu–Ni at the same temperature, due to the higher melting point of the latter. For example, the impurity diffusion coefficient of Zn in Al, extrapolated to the room temperature from the data of high temperature measurements is 4.7×10^{-26} m^2/s, which is by 18 orders of magnitude larger than D_{Cu}^{Ni} [95]. Taking into account the non-equilibrium defects produced during HPT decreases this enormous gap, but still the difference of several orders of magnitude remains.

The decomposition of the supersaturated (Co) solid solution [63] also needs the long-range diffusion of Co or Cu atoms. The diffusion can proceed through the bulk of material or along GBs and their triple junctions. The shortest diffusion path is half the distance, L, between fine Cu-particles in the as-processed Co alloys, namely 20 nm. All other possible diffusion lengths in the studied alloys are larger than 20 nm. For the bulk diffusion as a possible mechanism of the HPT-forced decomposition of the supersaturated solid solution, the simplest estimate is $L/2 = 2(D_{HPT}t)^{0.5}$, where t = 300 s is the duration of HPT treatment and D_{HPT} is the bulk diffusion coefficient. Then for L = 20 nm, $D_{HPT} = 5\times10^{-19}$ m^2/s. Extrapolation of D_b to 300 K for the bulk diffusion of Cu in Co gives $D_b = 10^{-41}$ m^2/s [100]. This discrepancy of more than 22 orders of magnitude clearly indicates

that the HPT treatment accelerates the atomic diffusion inside the processed material, probably due to intensive vacancy generation during deformation. These excess vacancies cannot be produced by conservative glide of Shockley partials. Therefore, a cross-slip and intensive interaction of dislocations occurs during HPT. The excess vacancies are produced as a result of dislocation reactions.

In the Cu-rich Cu–Co alloys [69], the Co precipitates in sample 1 (as described above) were partly dissolved during HPT, which was accomplished in a period of time of t = 300 s [69]. Let us suppose that this dissolution was controlled by the atomic diffusion. The diffusion path in this case would be equal to the distance between fine Co precipitates in Sample 1, i.e. d = 200 nm (right inset in Fig. 1a). It corresponds to the bulk diffusion coefficient of $D = 10^{-16}$ m^2/s. On the other hand, the extrapolation of the published results of diffusion measurements to the temperature of the current SPD treatment, T_{SPD}, T_{SPD} = 300 K gives $D = 10^{-38}$ m^2/s for diffusion of Co in Cu [101] and $D = 10^{-35}$ m^2/s for self-diffusion in Cu [102]. If we suppose that the mass transfer was controlled by the grain boundary (GB) diffusion, the extrapolation of the respective data to T_{SPD} reveals $D_{GB} = 10^{-19}$ m^2/s for Cu self-diffusion [103], $D_{GB} = 10^{-22}$ m^2/s for Ni GB diffusion in coarse-grained Cu polycrystals [104] and $D_{GB} = 10^{-19}$ m^2/s for Ni GB diffusion in nanograined Cu polycrystals [98] (D_{GB} for Co was not measured up to now). As seen, the discrepancy is high: the mass transfer during SPD (HPT in the current work) occurs from 3 to 12 orders of magnitude faster than any possible diffusion process can facilitate. Moreover, the applied pressure of 6 GPa additionally slows down the diffusion as well as GB migration [64, 65]. Therefore, we have to consider the deformation-driven mechanisms of mass transfer.

HPT of the Cu–13.5 at. % In alloy leads to the partial dissolution of δ-phase precipitates [70]. We can estimate the equivalent diffusion coefficient D_{HPT} for the results of this HPT-driven mass transfer from the simple equation $L = (D_{HPT}\, t)^{0.5}$, where t = 300 s (being the HPT duration) and L is the distance of the mass-transfer. The initial rarely positioned few-micrometer large precipitates were substituted by the fine particles of nanometer size. The shortest possible distance for this HPT-driven mass transfer is comparable with a matrix grain size L = 20 nm. Other estimations would give even larger values of L. Thus, $D_{HPT} = 10^{-18}$ m/s^{-2}. The extrapolation of D for Cu self diffusion and In bulk diffusion in Cu to 300 K (temperature of HPT treatment) gives $D = 10^{-35}$ m^2/s [102] and $D = 10^{-39}$ m/s^{-2} [105], respectively. Similar extrapolation of In GB diffusion coefficient gives $D_{GB} = 10^{-28}$ m/s^{-2} [106]. In spite of the fact that high pressure slows down both bulk and GB diffusion [64, 65], the D_{HPT} is 10 to 21 orders of magnitude higher than these extrapolated values.

For the Cu–Sn alloys we also can compare deformation-stimulated mass transfer and conventional thermal diffusion [71]. The bulk diffusion coefficient D_{HPT} necessary for such mass transfer can formally be estimated by the formula $L = (D_{HPT}\, t)^{0.5}$. The duration t of the high pressure torsion process is 300 s. The distance L at which mass transfer occurs can be estimated as half of the dimension of grains after high pressure torsion, i.e., $L \sim 100$ nm. Correspondingly, $D_{HPT} \sim 10$–17 m^2/s. The extrapolation of D for bulk self diffusion in copper to 300 K (temperature of high pressure torsion T_{HPT}) and bulk diffusion of tin in copper gives $D = 10^{-35}$ m^2/s [102] and $D = 10^{-31}$ m^2/s [106], respectively. Although the pressure reduces the bulk and grain boundary diffusion coefficients [64, 65], D_{HPT} is 14–18 orders of magnitude larger than these extrapolated values. This means that high pressure torsion strongly accelerates mass transfer as in our preceding experiments. Therefore, the equivalent diffusion coefficient for the SPD-driven mass transfer is comparable with the conventional diffusion coefficient at (elevated) T_{eff}.

Analysing and comparing all these results, one can conclude that the original idea of George Martin [1] is applicable, in its developed form, also to the SPD-driven phase transformations. We can draw this conclusion despite to the fact that in the model of G. Martin it is supposed that the irradiation-driven movements of atoms are similar to the diffusion jumps. This is, obviously, not completely true for the case of SPD-driven movements of atoms. Nevertheless, the general tendency (1) is quite similar. In this work we have compared the alloys deformed by HPT in comparable conditions ($T_{SPD} \sim$ 300K, ~ 5 GPa, ~ 1 rpm, ~ 5 torsions) with each other. One can suppose that the

SPD-driven atomic movements are comparable in all systems under consideration. On the other hand, the "natural" diffusion movements of the atoms are quite different due to the difference of melting temperature T_m of the considered materials. Since the T_{SPD} ~ 300K is almost the same, the "natural" diffusion coefficients are low for the materials with high T_m. In this case the SPD-driven atomic movements are large in comparison with diffusion jumps, and T_{eff} is high (as predicted by G. Martin, see the eq. (1)). In the opposite case of low T_m (like in the Al-based alloys), the T_{eff} is low and can be close to the ambient temperature of T_{SPD} [13, 14]. SPD also accelerates the mass transfer in the materials. Frequently the equivalent diffusion coefficient for the SPD-driven mass transfer is comparable with the conventional diffusion coefficient at (elevated) T_{eff}.

Summary

Severe plastic deformation by HPT leads to the phase transitions and strong grain refinement in several metallic alloys. SPD-treatment at ambient temperature T_{SPD} is frequently equivalent to the heat treatment at a certain elevated (effective) temperature T_{eff}. If the condition of SPD-treatment are similar, the materials with high melting temperature T_m also yield high T_{eff} values. The materials with low T_m have low T_{eff}. SPD also accelerates the mass transfer in the materials. Frequently the equivalent diffusion coefficient for the SPD-driven mass transfer is comparable with the conventional diffusion coefficient at (elevated) T_{eff}.

Acknowledgements

The work was partially supported by the Russian Foundation for Basic Research (grants 14-48-03598, 14-03-31510, 14-08-00972 and 15-03-01127), Government of Moscow Region, the Russian Federal Ministry for Education and Science (grants 14.A12.31.0001 and Increase Competitiveness Program of NUST «MISiS» К2-2014-013; RZV through the Russian Program "5-100-2020" at Research Laboratory for Mechanics of New Nanomaterials, St Petersburg State Polytechnical University), Karlsruhe Nano Micro Facility, The Allianz Industrie Forschung (grant FE.5150.0028.4067), and Polish National Science Centre (grant DEC-2011/01/M/ST8/07822).

References

[1] R.Z. Valiev, R.K. Islamgaliev, I.V. Alexandrov, Progr. Mater. Sci. 45 (2000) 103–189.

[2] E.I. Teitel', L.S. Metlov, D.V. Gunderov, A.V. Korznikov, Phys. Metall. Metallogr. 113 (2012) 1162–1168.

[3] X. Sauvage, A. Chbihi, X. Quelennec, J. Phys. 240 (2010) 012003.

[4] H.W. Zhang, S. Ohsaki, S. Mitao, A. Ohnuma, K. Hono, Mater. Sci. Eng. A 421 (2006) 191–199.

[5] W. Lojkowski, M. Djahanbakhsh, G. Burkle, S. Gierlotka, W. Zielinski, H.J. Fecht, Mater. Sci. Eng. A 303 (2001) 197–208.

[6] K. Hono, M. Ohnuma, M. Murayama, S. Nishida, A. Yoshie, T. Takahashi, Scripta Mater. 44 (2001) 977–983.

[7] A. Taniyama, T. Takayama, M. Arai, T. Hamada, Scripta Mater. 51 (2004) 53–58.

[8] V.G. Gavriljuk, Mater. Sci. Eng. A 345 (2003) 81–89.

[9] X. Sauvage, X. Quelennec, J.J. Malandain, P. Pareige, Scripta Mater. 54 (2006) 1099–1103.

[10] V.A. Teplov, V.P. Pilugin, V.S. Gaviko, E.G. Chernyshov, Phil. Mag. B 68 (1993) 877–881.

[11] V.V. Stolyarov, R. Lapovok, I.G. Brodova, P.F. Thomson, Mater. Sci. Eng. A 357 (2003) 159–167.

[12] X. Sauvage, F. Wetscher, P. Pareige, Acta Mater. 53 (2005) 2127–2135.

[13] B.B. Straumal, B. Baretzky, A.A. Mazilkin, F. Phillipp, O.A. Kogtenkova, M.N. Volkov, R.Z. Valiev, Acta Mater. 52 (2004) 4469–4478.

[14] A.A. Mazilkin, B.B. Straumal, E. Rabkin, B. Baretzky, S. Enders, S.G. Protasova, O.A. Kogtenkova, R.Z.Valiev, Acta Mater. 54 (2006) 3933–3939.

[15] B.B. Straumal, S.G. Protasova, A.A. Mazilkin, E. Rabkin, D. Goll, G. Schütz, B. Baretzky, R.Z. Valiev, J. Mater. Sci. 47 (2012) 360–367.

[16] C.M. Cepeda-Jiménez, J.M. García-Infanta, A.P. Zhilyaev, O.A. Ruano, and F. Carreño, J. Alloys Comp. 509 (2011) 636–643.

[17] Y. Ivanisenko, I. MacLaren, X. Sauvage, R.Z. Valiev, H.-J. Fecht, Acta Mater. 54 (2006) 1659–1669.

[18] X. Sauvage, Y. Ivanisenko, J. Mater. Sci. 42 (2007) 1615–1621.

[19] Y. Ivanisenko, W. Lojkowski, R.Z. Valiev, H.J. Fecht, Acta Mater. 51 (2003) 5555–5570.

[20] V.V. Sagaradze, S.V. Morozov, V.A. Shabashov, L.N. Romashev, R.I. Kuznetsov, Phys. Met. Metall. 66 (1988) 328–338.

[21] B.B. Straumal, A.A. Mazilkin, S.G. Protasova, S.V. Dobatkin, A.O. Rodin, B. Baretzky, D. Goll, G. Schütz, Mater. Sci. Eng. A 503 (2009) 185–189.

[22] V.V. Sagaradze, V.A. Shabashov, Nanostruct. Mater. 9 (1997) 681–684.

[23] M. Murayama, K. Hono, Z. Horita, Mater. Trans. – JIM 40 (1999) 938–941.

[24] S. Ohsaki, S. Kato, N. Tsuji, T. Ohkubo, K. Hono, Acta Mater. 55 (2007) 2885–2895.

[25] X. Sauvage, R. Pippan, Mater. Sci. Eng. A 410–411 (2005) 345–347.

[26] X. Sauvage, C. Genevois, G. Da Costa, V. Pantsyrny, Scripta Mater. 61 (2009) 660–663.

[27] X. Sauvage, W. Lefebvre, C. Genevois, S. Ohsaki, K. Hono, Scripta Mater. 60 (2009) 1056–1061.

[28] B.B. Straumal, S.V. Dobatkin, A.O. Rodin, S.G. Protasova, A.A. Mazilkin, D. Goll, B. Baretzky, Adv. Eng. Mater. 13 (2011) 463–469.

[29] A.V. Korznikov, O. Dimitrov, G.F. Korznikova, J.P. Dallas, A. Quivy, R.Z. Valiev, A. Mukherjee, Nanostruct. Mater. 11 (1999) 17–23.

[30] A.V. Korznikov, G. Tram, O. Dimitrov, G.F. Korznikova, S.R. Idrisova, Z. Pakiela, Acta Mater. 49 (2001) 663–671.

[31] C. Rentenberger, H.P. Karnthaler, Acta Mater. 56 (2008) 2526–2530.

[32] A.V. Sergueeva, C. Song, R.Z. Valiev, A.K. Mukherjee, Mater. Sci. Eng. A 339 (2003) 159–165.

[33] S.D. Prokoshkin, I.Yu. Khmelevskaya, S.V. Dobatkin, I.B. Trubitsyna, E.V. Tatyanin, V.V. Stolyarov, E.A. Prokofiev, Acta Mater. 53 (2005) 2703–2714.

[34] X. Sauvage, L. Renaud, B. Deconihout, D. Blavette, D. H. Ping, K. Hono, Acta. Mater. 49 (2001) 389–394.

[35] T. Miyazaki, D. Terada, Y. Miyajima, C. Suryanarayana, R. Murao, Y. Yokoyama, K. Sugiyama, M. Umemoto, T. Todaka, N. Tsuji, J. Mater. Sci. 46 (2011) 4296–4301.

[36] A.A. Mazilkin, G.E. Abrosimova, S.G. Protasova, B.B. Straumal, G. Schütz, S.V. Dobatkin, A.S.Bakai, J. Mater. Sci. 46 (2011) 4336–4342.

[37] V.V. Stolyarov, D.V. Gunderov, A.G. Popov, V.S. Gaviko, A.S. Ermolenko, J. Alloys Comp. 281 (1998) 69–71.

[38] Y. Matsuura, S. Hirosawa, H. Yamamoto, S. Fujimira, M. Sagawa, K. Osamura, Jap. J. Appl. Phys. Part 2 – Lett. 24 (1985) L635– L637.

[39] B.B. Straumal, A.A. Mazilkin, S.G. Protasova, D. Goll, B. Baretzky, A.S. Bakai, S.V. Dobatkin, Kovove Mater. – Metall. Mater. 49 (2011) 17–22.

[40] Á. Révész, S. Hóbor, J.L. Lábár, A.P. Zhilyaev, Zs. Kovácz, J. Appl. Phys.100 (2006) 103522.

[41] I. MacLaren, Y. Ivanisenko, R.Z. Valiev, H.J. Fecht, J. Phys. 26 (2006) 335–338.

[42] Y. Ivanisenko, I. MacLaren, X. Sauvage, R.Z. Valiev, H.J. Fecht, Sol. State Phen. 114 (2006) 133–144.

[43] Y. Ivanisenko, I. MacLaren, X. Sauvage, R.Z. Valiev, H.J. Fecht, Acta Mater. 54 (2006) 1659–1669.

[44] A.P. Zhilyaev, I. Sabirov, G. González-Doncel, J. Molina-Aldareguía, B. Srinivasarao, M.T. Pérez-Prado, Mater. Sci. Eng. A 528, (2011) 3496–3505.

[45] A.P. Zhilyaev, A.V. Sharafutdinov, M.T. Pérez-Prado, Adv. Eng. Mater. 12 (2010) 754–757.

[46] A.P. Zhilyaev, F. Gálvezc, A.V. Sharafutdinov, M.T. Pérez-Prado, Mater. Sci. Eng. A 527 (2010) 3918–3928.

[47] M.T. Pérez-Prado, A.V. Sharafutdinov, A.P. Zhilyaev, Mater. Lett. 64, (2010) 211–214.

[48] M.T. Pérez-Prado, A.P. Zhilyaev, Phys. Rev. Lett. 102 (2009) 175504.

[49] K. Edalati, Z. Horita, Y. Mine, Mater. Sci. Eng. A 527 (2010) 2136–2141.

[50] K. Edalati, Z. Horita, S. Yagi, E. Matsubara, Mater. Sci. Eng. A 523 (2009) 277–281.

[51] K. Edalati, E. Matsubara, Z. Horita, Metal Mater Trans A 40 (2009) 2079–2086.

[52] Y. Ivanisenko, A. Kilmametov, H. Roesner, R.Z. Valiev, Int. J. Mater. Res. 99 (2008) 36–41.

[53] A.M. Glezer, M.R. Plotnikova, A.V. Shalimova, S.V. Dobatkin, Bull. Russ. Ac. Sci. Phys. 73, (2009) 1233–1236.

[54] S. Hóbor, Á. Révész, A.P. Zhilyaev, Zs. Kovácz, Rev. Adv. Mater. Sci. 18 (2008) 590–592.

[55] Zs. Kovács, P. Henits, A.P. Zhilyaev, Á.Révész, Scripta Mater. 54 (2006) 1733–1737.

[56] G.E. Abrosimova, A.S. Aronin, S.V. Dobatkin, S.D. Kaloshkin, D.V. Matveev, O.G. Rybchenko, E.V. Tatyanin, I.I. Zverkova, J. Metastab. Nanocryst. Mater. 24, (2005) 69–72.

[57] Á. Révész, E. Schafler, Zs. Kovács, Appl. Phys. Lett. 92 (2008) 011910.

[58] S. Hóbor, Zs. Kovács, A.P. Zhilyaev, L.K. Varga, P. J. Szabó, Á. Révész, J. Phys. 240, 012153 (2010).

[59] S. Hóbor, Á. Révész, P. J. Szabó, A.P. Zhilyaev, V. Kovács Kis, J.L. Lábár, Zs. Kovács, J. Appl. Phys. 104 (2008) 033525.

[60] P. Henits, Á. Révész, A.P. Zhilyaev, Zs. Kovács, J. Alloys Comp. 461, (2008) 195–199.

[61] Zs. Kovács, P. Henits, A.P. Zhilyaev, N.Q. Chinh, Á. Révész, Mater. Sci. Forum 519-521 (2006) 1329–1334.

[62] G. Martin, Phys. Rev. B 30 (1984) 1424–1436.

[63] B.B. Straumal, A.A. Mazilkin, B. Baretzky, E. Rabkin, R.Z. Valiev, Mater. Trans. 53 (2012) 63–71.

[64] B. B. Straumal, L. M. Klinger, L. S. Shvindlerman, Scripta metall. 17, (1983) 275–279.

[65] D.A. Molodov, B.B. Straumal, L.S. Shvindlerman, Scripta metal. 18, (1984) 207–211.

[66] G. Thomas, H. Mori, H. Fujita, Scripta Metall. 16, (1982) 589–592.

[67] A.A. Mazilkin, B.B. Straumal, M.V. Borodachenkova, R.Z. Valiev, O.A. Kogtenkova, B. Baretzky, Mater. Lett. 84 (2012) 63–65.

[68] T.B. Massalski (Ed.), Binary Alloy Phase Diagrams, 2nd ed., ASM International, Materials Park, OH, 1990.

[69] B.B. Straumal, A.R. Kilmametov, Yu.O. Kucheev, L. Kurmanaeva, Yu. Ivanisenko, B. Baretzky, A. Korneva, P. Zięba, D.A. Molodov, Mater. Lett. 118 (2014) 111–114.

[70] B.B. Straumal, A.R. Kilmametov, A.A. Mazilkin, L. Kurmanaeva, Y. Ivanisenko, A. Korneva, P. Zięba, B. Baretzky, Mater. Lett. 138 (2014) 255–258.

[71] B.B. Straumal, A.R. Kilmametov, Yu. O. Kucheev, K.I. Kolesnikova, A. Korneva, P. Zięba, B. Baretzky, JETP Lett. 100 (2014) 376–379

[72] B.B. Straumal, A.R. Kilmametov, Yu. Ivanisenko, A.A. Mazilkin, O.A. Kogtenkova, L. Kurmanaeva, A. Korneva, P. Zięba, B. Baretzky, Int. J. Mater. Res. (former Zt. Metallkunde) 106 (2015) in press.

[73] G. Thomas, H. Mori, H. Fujita, Scr. Metal. 16 (1982) 589–592.

[74] Z.S. Ji, M.L. Hu, X.P. Zheng, J. Mater. Sci. Technol. 23 (2007) 247–252.

[75] Y.A. Shatilla, E.P. Loewen, Nucl. Technol. 151 (2005) 239–249.

[76] M. Sagawa, S. Fujimura, N. Togawa, H. Yamamoto, Y. Matsuura, J. Appl. Phys. 55 (1984) 2083–2087.

[77] U.R. Kattner, JOM 49(12) (1997) 14–19.

[78] N. Mattern, U. Kühn, A. Gebert, A. Schoeps, T. Gemminga, L. Schultz, Mater. Sci. Eng. A 449/451 (2007) 207–210.

[79] I. Gödény, D.L. Beke, F.J. Kedves, Phys. Stat. Sol. A 13 (1972) K155– K157.

[80] N.L. Peterson, S.J. Rothman, Phys. Rev. B 1 (1970) 3264–3272.

[81] S.J. Rothman, N.L. Peterson, L.J. Nowicki, L.C. Robinson, Phys. Stat. Sol. B 63 (1974) K29–K33.

[82] G. Saada, Acta Met. 9 (1961) 965–975.

[83] D.L. Beke, I. Gödény, F.J. Kedves, Phil. Mag. A. 47 (1983) 281–299.

[84] D.L. Beke, I. Gödény, F.J. Kedves, Trans. Jap. Inst. Met. Suppl. 27 (1986) 649–653.

[85] A.N. Aleshin, V.Yu. Aristov, B.S. Bokstein, L.S. Shvindlerman, Phys. Stat. Sol. A 45 (1978) 359–366.

[86] A.N. Aleshin, B.S. Bokstein, A.L. Petelin, L.S. Shvindlerman, Metallofiz. 2 (1980) 83–95.

[87] P. Zieba, A. Pawlowski, W. Gust, Def. Diff. Forum 194 (2001) 1759–1765.

[88] A. Häßner, Isotopenpraxis 5 (1969) 143–149.

[89] A. Häßner, Krist. Tech. 8 (1973) K1–K11.

[90] A. Häßner, Krist. Tech. 9 (1974) 1371–1379.

[91] T. Fujita, H. Hasegawa, Z. Horita, T.G. Langdon, Def. Diff. Forum 194 (2001) 1205–1210.

[92] T. Fujita, Z. Horita, T.G. Langdon, Phil. Mag. A 82 (2002) 2249–2262.

[93] T. Fujita, Z. Horita, T.G. Langdon, Mater. Sci. Forum 396 (2002) 1061–1066.

[94] A.B. Vladimirov, V.N. Kaygorodov, S.M. Klotsman, V.D. Symbelov, I.S. Trachtenberg, Phys. Metal. Metallogr. 39 (1) (1975) 78–82.

[95] H. Mehrer (Ed.), Diffusion in Solid Metals and Alloys, Landolt-Börnstein New Series, Gr III, Vol. 26, Springer-Verlag, Berlin, 1990.

[96] H.-E. Schaefer, Phys. Stat. Sol. A 102 (1987) 47–65.

[97] S.V. Divinski, G. Reglitz, H. Rösner, Y. Estrin , G. Wilde, Acta. Mater. 59 (2011) 1974–1985.

[98] Y. Amouyal, S.V. Divinski, Y. Estrin, E. Rabkin, Acta Mater. 55 (2007) 5968–5979.

[99] P. Bellon, R.S. Averback, Phys. Rev. Lett. 74 (1995) 1819–1822.

[100] G. Neumann, V. Tolle, Phil. Mag. A 57 (1988) 621–630.

[101] C.A. Mackliet, Phys. Rev. 109 (1958) 1964–1970.

[102] S. Fujikawa, K.I. Hirano, in: J.I. Takamura, M. Doyama, M. Kiritani (Eds.) Proc. of Yamada Vth Conf. on Point Defects, Defect Interactions in Metals, Univ. of Tokyo Press, Tokyo, 1982, pp. 554–558.

[103] T. Surholt, Chr. Herzig, Acta Mater. 45 (1997) 3817–3823.

[104] S. Divinski, J. Ribbe, G. Schmitz, Chr. Herzig, Acta Mater. 55 (2007) 3337–3346.

[105] V.A. Gorbachev, S.M. Klotsman, Ya.A. Rabovskiy, V.K. Talinskiy, A.N. Timofeyev, Phys. Met. Metallogr. 34(4) (1972) 202–206.

[106] W. Gust, B. Predel, U. Roll, Acta Metall. 28 (1980) 1395–1405.